Influence of Ship Motion on Flow Field over Modified Simple Frigate Shapes

*LI Tong, WANG Yibin, ZHAO Ning**

Key Laboratory of Unsteady Aerodynamics and Flow Control, Ministry of Industry and Information Technology, Nanjing University of Aeronautics and Astronautics, Nanjing 210016, P. R. China

(Received 10 June 2020; revised 20 July 2020; accepted 1 September 2020)

Abstract: When the frigate moves forward, due to the ship motion such as pitching and rolling, the flow over the flight deck becomes very complex, which may seriously threaten the taking off and landing of the ship-borne helicopter. The flow fields over the different modified simple frigate shape (SFS) models, consisting of the hangar and flight deck, were numerically studied by changing the ratio of hangar height and length in the static state and pitching state. For different models, the contours of velocity and pressure above the flight deck, as well as the variations of velocity components of the observation points and line in static state and pitching state were compared and analyzed. The results show that the size of recirculation zone and the location of the reattachment point have distinct differences for diverse models, and reveal the tracks of recirculation zone's center and reattachment position in a pitching period. In addition, the velocity components at two observation positions also change periodically with the periodic motion. Furthermore, the deviations of the velocity components in static state and pitching state are relatively large, therefore, the flow fields in static state cannot be used to simulate that in pitching state correctly.

Key words: computational fluid dynamics; simple frigate shape; ship airwake; pitching; recirculation zone

CLC number: V211.3 **Document code:** A **Article ID:** 1005-1120(2021)03-0520-15

0 Introduction

Air passing through the ship's superstructure causes the formation of a region of disturbed flow over the flight deck due to a combination of its forward speed and the prevailing wind, which is known as the ship airwake[1]. The flight deck is the main site for the ship-borne helicopter operations over the sea, and the flow over the deck is significantly affected by natural wind, superstructure shape and ship motion. When the frigate moves forward, the ship airwake appears in the rear of the hangar, accompanying with the flow separation, backflow and vortex. Meanwhile, due to the different wind over deck (WOD) and movement such as heaving, pitching and rolling, the flow over the flight deck becomes very complex, which may seriously threaten the taking off and landing of the ship-borne helicopter. Therefore, there must be a clear understanding of the characteristics of the ship airwake over the flight deck.

In the early years, the wind tunnel model test and in situ experiment were main methods to study the ship airwake over the flight deck. In 1992, since the previous simulator was based on a faulty airwake database, which was based on a uniform velocity profile and very low turbulence, Healey attempted to correct this situation by making three-dimensional hot-wire anemometer measurements of the airwake properties of a stationary 1/141-scale model ship in a simulated atmospheric boundary layer[2]. In 2014, Bardera-Mora presented the main results of the ship airwake simulation performed on a frigate ship model in a low-speed wind tunnel by particle image velocimetry (PIV)[3]. Moreover, wind velocity measurements on board above the flight

*Corresponding author, E-mail address: zhaoam@nuaa.edu.cn.

How to cite this article: LI Tong, WANG Yibin, ZHAO Ning. Influence of ship motion on flow field over modified simple frigate shapes[J]. Transactions of Nanjing University of Aeronautics and Astronautics, 2021, 38(3): 520-534.

http://dx.doi.org/10.16356/j.1005-1120.2021.03.016

deck were also carried out by a sonic anemometer and results were compared with these obtained in wind tunnel tests. The results show that the turbulence intensity levels measured on board are lower than these measured in the wind tunnel tests. These differences can be probably due to differences in the boundary layer parameters (velocity profile and spectrum). However, these two methods require lots of manpower and resources, and are also very time consuming. In the recent years, the computational fluid dynamics (CFD) method has been gradually developed and widely used to research the ship airwake over the flight deck. The unsteady flow field of an LHA-class U.S. Navy ship was simulated numerically by Polsky in 2002[4], and the results were compared well with both wind tunnel and in situ experiment data. The research on the airwake simulation for a Navy destroyer DDG-81 was performed by Woodson and Ghee in 2005[5], which indicated that the CFD methods could successfully simulate ship airflow. Later, Thornber et al. studied two different Royal Navy ships for fourteen different wind angles with implicit large eddy simulation (ILES)[6]. The study for evaluating the aerodynamic impact of ship superstructures on helicopter operations was performed by Kääriä et al. in 2013[7]. Compared to the baseline ship geometry, all the ship modifications, particularly the side-flap and the notch modification, can significantly reduce root-mean-square forces and moments. Lately, Watson et al. performed the computational and experimental modeling study of the unsteady airflow over the United Kingdom's new aircraft carrier HMS Queen Elizabeth[8]. Their full-scale CFD results showed reasonable agreement with the small scale experiment results, suggesting that the full-scale CFD method is at least as representative of the full-scale situation as the small-scale experiment. Therefore, the CFD method can be used to simulate the flow field over the large ship and offer correct flow data for pilots.

Under the auspices of the technical co-operation programmer(TTCP), a collaborative ship airwake modeling activity was set up to develop a ship airwake validation database[9]. Therefore, the simple frigate shape (SFS) and its updated version SFS2 shown in Fig.1 were created to provide an easy research on the ship airwake. The simple SFS is a highly simplified ship geometry, which was created originally by a ship airwake modeling working group within TTCP. Later, the National Research Council of Canada (NRC) performed a series of wind tunnel experiments on both geometries[10-11]. The steady-state ship airwake over the SFS was also numerically studied with commercial software Fluent[12], which showed that the general features of the flow compare reasonably well between the experimental data and predicted data. Syms used the Lattice-Boltzmann method to investigate the flow topology on and off the surface of the SFS[13]. Because of the ability in capturing the turbulent structures for massively separated flow, the detached-eddy simulation (DES) turbulence model[14], as well as its improved versions delayed DES (DDES)[15] and improved DDES (IDDES)[16], becomes a popular turbulence model for the ship airwake researches. In 2010, Forrest et al. numerically studied the ship airwake of the SFS2 and a Royal Navy Type 23 Frigate with DES method[1]. Comparisons of DES results and wind tunnel data showed good agreement, which indicated that the DES method can be used to simulate the ship airwake. Zhao et al. employed the entropy-based detached-eddy simulation (SDES) method to simulate the airwake on SFS model, and concluded that SDES could accurately predict airwake[17]. Li et al. found that both large-eddy simulation (LES) result and DES result all well match the experimental result[18]. Moreover, they found that both LES and DES methods are superior to RANS method in simulating ship airwake. The DDES method was used to compute the unsteady ship airwake on the SFS2 as well as the Canadian Patrol Frigate, and the results were well compared with the experimental results[19]. Lately, a parametric study, employing IDDES with the shear stress transport (SST) k-ω turbulence model, was conducted by varying the hangar length to find the optimal afterbody model with minimal recirculation zone behind the hangar, and the optimal afterbody model was obtained[20].

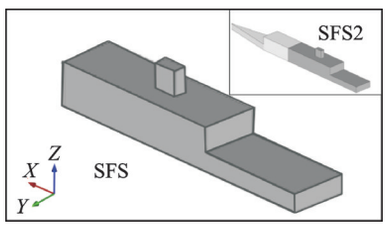

Fig.1 Schematic of SFS and its updated version SFS2

However, most of the researches on the flow fields of SFS and SFS2 were based on the motionless state, without considering the ship motion caused by the sea waves. In this paper, the flow fields over the modified SFS models with different hangar's geometries were numerically simulated in both static state and motion state. The purpose of this study is to investigate the effect of the motion state and different hangar's geometries on the flow fields over the helideck.

1 Numerical Method

Since the inflow Mach number is less than 0.3, thus the flow around the ship can be treated as the incompressible flow. The incompressible flow governing equations are

$$\nabla \cdot \boldsymbol{V} = 0 \tag{1}$$

$$\rho(\mathrm{d}\boldsymbol{V}/\mathrm{d}t) + \nabla p = \boldsymbol{F} \tag{2}$$

where $\boldsymbol{V}$ is the velocity vector, ρ the density of the air, $\mathrm{d}\boldsymbol{V}/\mathrm{d}t$ the material derivative of $\boldsymbol{V}$, p the static pressure, and $\boldsymbol{F}$ the viscous force vector. The commercial CFD solver FLUENT was used for the numerical simulation, employing RANS with the k-ε turbulence model for closure. The coupling of the pressure and velocity was handled using semi-implicit method for pressure-linked equation (SIMPLE) algorithm and the time discretization was performed implicitly using a second-order accurate scheme with dual time stepping.

The dynamic mesh method was used to deform the mesh thus to simulate the ship's motion. The spring-based smoothing, used in this paper, is one of the dynamic mesh updated method, where the edges between any two mesh nodes are idealized as a network of interconnected springs. The initial spacings of the edges before any boundary motion constitute the equilibrium state of the mesh. A displacement at a given boundary node will generate a force proportional to the displacement along all the springs connected to the node. Using Hook's Law, the force on a mesh node can be written as

$$\boldsymbol{F}_i = \sum_j^{n_i} k_{ij}(\Delta \boldsymbol{x}_j - \Delta \boldsymbol{x}_i) \tag{3}$$

where $\Delta \boldsymbol{x}_i$ and $\Delta \boldsymbol{x}_j$ are the displacements of node i and its neighbor j. n_i is the number of neighboring nodes connected to node i, and k_{ij} the spring constant between node i and its neighbor j.

The spring constant for the edge connecting nodes i and j is defined as

$$k_{ij} = k_{\mathrm{fac}} \Big/ \sqrt{|\boldsymbol{x}_i - \boldsymbol{x}_j|} \tag{4}$$

where k_{fac} is the value for spring constant factor. At equilibrium, the net force on a node due to all the springs connected to the node must be zero. This condition results in an iterative equation such that

$$\Delta \boldsymbol{x}_i^{m+1} = \left(\sum_j^{n_i} k_{ij} \Delta \boldsymbol{x}_j^m \right) \Big/ \sum_j^{n_i} k_{ij} \tag{5}$$

where m is the iteration number.

Since the displacements are known at all the boundaries (after boundary node positions have been updated), Eq.(5) is solved using a Jacobi sweep on all interior nodes. At convergence, the positions are updated such that

$$\boldsymbol{x}_i^{n+1} = \boldsymbol{x}_i^n + \Delta \boldsymbol{x}_i^{\mathrm{converged}} \tag{6}$$

2 Model and Grid

The SFS is a representative case of the study on the flow over the ship flight deck, since it has a simplified geometry containing the hangar, bridge (funnel/mast) and flight deck (shown in Fig.1). The configuration used in this study was shown in Fig.2. It is a modified SFS model named MSFS without the bridge on the hangar, which also can be regarded as the simplified afterbody of frigate. Some preliminary tests were undertaken with and without the bridge, and their results found that the bridge has relatively little effect on the aft flow field[21]. Therefore, the bridge on the SFS was removed in this paper for convenience.

The multi-block structured grid of the MSFS was shown in Fig.3, and the enlarged view of grid

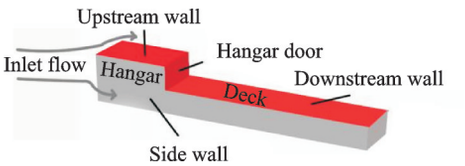

Fig.2 Schematic of MSFS geometry model

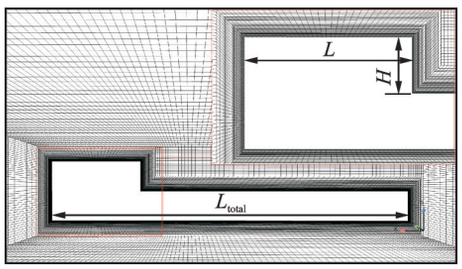

Fig.3 Schematic of grid at the central section

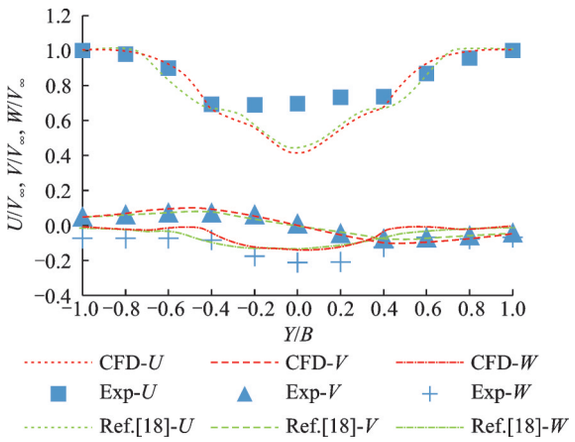

Fig.4 Comparison of experiment data and RANS results

was shown at the top right corner of graph. The velocity inlet boundary is in front of the flow field, and the velocity magnitude of the freestream is 10 m/s. The pressure outlet boundary is in the rear. The width of the hangar is set to B, the height is H, and the length is L, where B= 0.1 m, H=0.05 m. R is defined as H/L and the total length L_{total}=12H. In this paper, by changing the height-length ratio R, the flow fields of different MSFS models for a headwind were numerically studied in the static state and motion state (pitching and rolling), respectively. For convenience, the MSFS models with R=1∶1, R=1∶3 and R=1∶6 are named $M1$, $M3$ and $M6$, respectively.

3 Verification Process

To verify the numerical method, the numerical simulation results of the SFS2 model were compared with experimental data. The normalized velocity components along a lateral line were shown in Fig.4, where U, V, W denote longitudinal velocity in the X direction, lateral velocity in the Y direction and vertical velocity in the Z direction, respectively. The lateral position is normalized by the ship beam. The results in this study are consistent with the numerical results of Li et al.[18], which are also used the RANS turbulent model. For the both RANS results, the velocity components are well matched with the experimental data[1] except the longitudinal velocity near the center of the line. The reason for this discrepancy is that the velocity fluctuation behind the hangar is averaged by RANS model. Though there is a discrepancy between experiment data and RANS results, Reddy et al. have demonstrated the feasibility of the numerical simulation of ship airwake with RANS k-ε turbulence model[12].

In order to verify the rationality and independence of the grid, the flow field of MSFS3 with approximately 2.6 million, 6 million and 11.5 million grid cells were numerically simulated and compared.

In Fig.5, the result was shown by plotting limiting streamlines (skin-friction lines) on the deck surface of the MSFS3. The limiting streamlines are the streamlines close to the surface, which can provide a lucid description of the flow topology. It can be clearly seen that the reattachment line on the deck surface is like a parabola. The recirculation zone is on its left side and the red line passes its apex. It also can be observed that the locations of the reattachment lines for different grids are basically same.

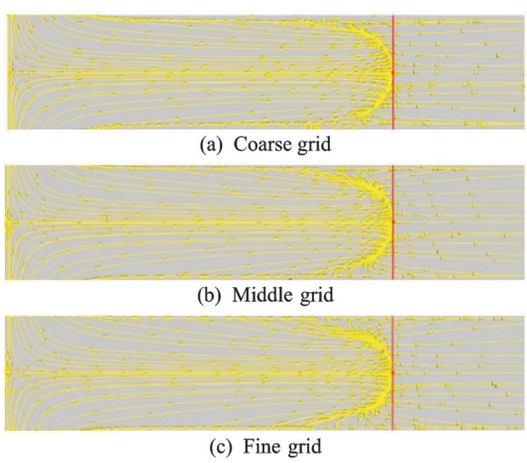

Fig.5 Limiting streamlines on MSFS deck surface

As can be seen from Table 1, for three different grids, the force coefficients in the same direction have only slight differences, which means that the calculation results are basically the same for different grids. Therefore, the coarse grid was used in this paper to improve the computational efficiency.

Table 1 Force coefficients of different directions for different grids

Direction	Coarse	Middle	Fine
X	0.907	0.898	0.895
Y	−0.000 002 85	0.000 572	0.000 002 33
Z	0.073	0.074	0.072

4 Result and Analysis

The numerical simulations were performed on the flow field of the different MSFS models in static state and pitching state in current study, respectively. The contours of velocity and pressure as well as the streamlines were compared and analyzed. Furthermore, the quantitative analysis of velocity components at the observation points and the observation line above the deck for different models was given. The positions of two observation points P_0 and P_1, colored in white and black, were shown in Fig.6. P_0 is located in the longitudinal central section and P_1 is on the left side of P_0, and they are both at 1/2 hangar height. The observation line (colored in red) and three different maps were shown in Fig.7. The line is parallel to Y direction and passes through P_0 and P_1.

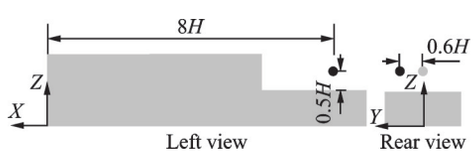

Fig.6 Schematic of observation points

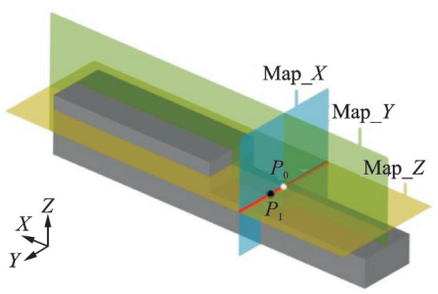

Fig.7 Schematic of observation line and maps

4.1 Static state

The numerical simulations of the flow fields over the MSFS models with different height-length ratios (R=1∶1, 1∶3, 1∶6, respectively) in the static state were carried out first, and the characteristics of the flow fields over the deck were analyzed and compared.

As seen in Fig.8, when the incoming flow passes the edge of MSFS front wall, the upstream recirculation zone A and downstream recirculation zone C with a clockwise rotation are formed due to the flow separation. The shear layer and the center of recirculation zone are located in the low speed area (colored in blue). After the flow reaches the downstream wall, the reattachment zone is formed. Meanwhile, the flow is divided into two parts. One part flows downstream and the other part goes upstream. When encountering the hangar door, it flows along the hangar door. After bypassing the edge of hangar door, a small upstream recirculation zone B with an anticlockwise rotation is generated for $M1$ and $M3$ models.

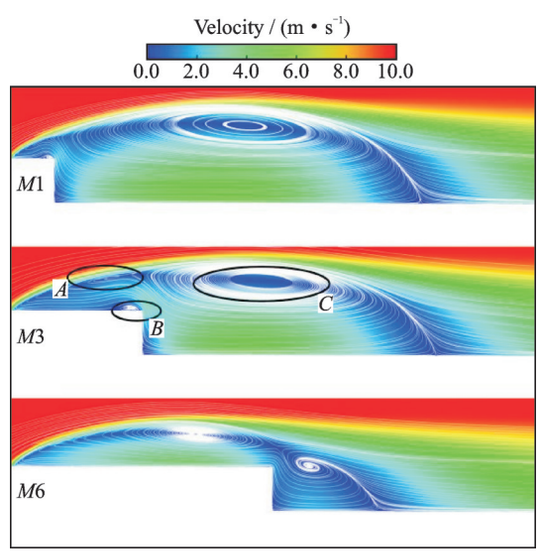

Fig.8 Contours of velocity and streamlines at Map_Y

For different models, the structures of flow fields have obvious discrepancy. There are two small upstream recirculation zones and one large downstream recirculation zone for the $M1$ and $M3$ models, while there are only two distinct recirculation zones for the $M6$ model, including one upstream recirculation zone A and one downstream re-

circulation zone C. With the increment of L, the upstream recirculation zone A increases, while the downstream recirculation zone C shrinks. The reason is that when the hangar length increases, there is enough space to form a large recirculation zone upstream, and more backflow is attached to the upstream wall, making the kinetic energy of the flow reduced due to the skin-friction. Consequently, the downstream recirculation zone becomes smaller because there is less energy to drive the flow to cycle in the downstream recirculation zone.

Fig.9 shows the flow structures for different models at horizontal plane Map_Z. Due to the headwind and symmetrical geometry, the flow fields on the left side and right side of different MSFS models are symmetrical. Similar to the contours of velocity and streamlines at Map_Y, on the one side of the MSFS, there are also two small upstream recirculation zones and one large downstream recirculation zone for $M1$ and $M3$ models, and only two distinct recirculation zones for $M6$ model. With the increase of L, the upstream recirculation zone D increases, too, while the downstream recirculation zone F shrinks.

The pressure distributions are diverse for different models in Fig.10. As can be seen that the downstream high pressure area (colored in yellow) in $M6$ is closer to the hangar door and the upstream low pressure area (colored in blue) is larger than that in $M1$. The downstream reattachment position is affected by high pressure area. Therefore, the size of downstream recirculation zone is limited by the location of high static pressure area.

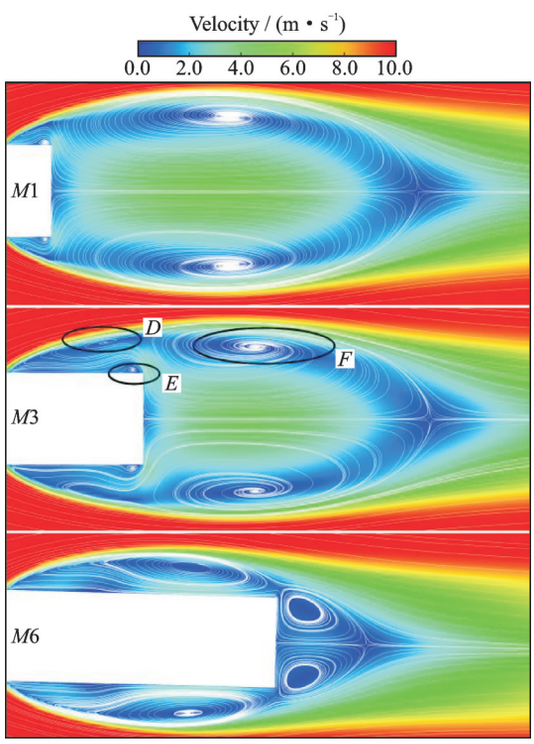

Fig.9 Contours of velocity and streamlines at Map_Z

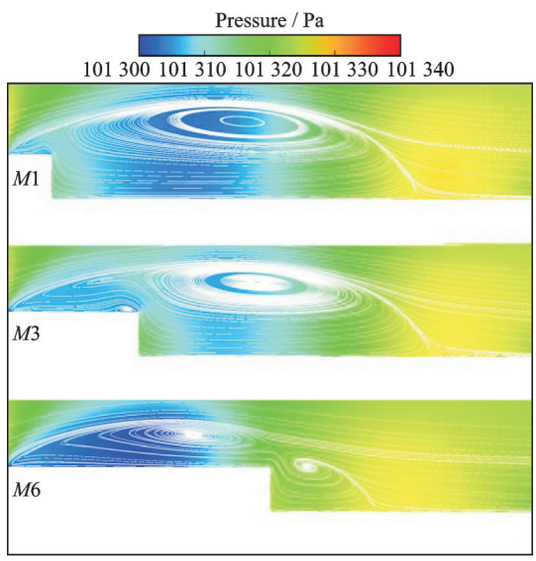

Fig.10 Contours of pressure and streamlines at Map_Y

The limiting streamline distributions on the downstream wall were given in Fig.11, and the left end is the location of hangar door. The locations of the reattachment lines for different models are diverse. However, the reattachment line on the deck surface for each model is all like a parabola. The recirculation zone is on its left side and the red line passes its apex. The length of downstream recirculation zone for $M6$ is denoted by L_d, and the result shows that the length of downstream recirculation

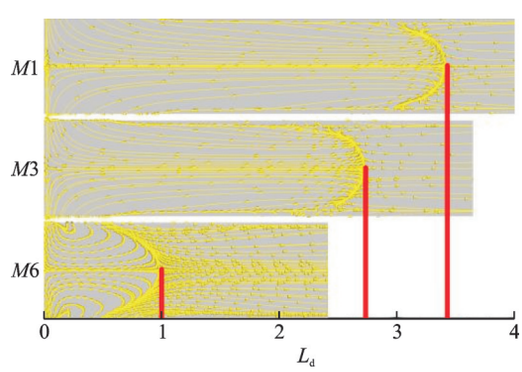

Fig.11 Streamlines distribution on downstream wall

zone for $M1$ and $M3$ is about $3.45L_d$ and $2.75L_d$, respectively. For a ship-borne helicopter, it is conducive to take off and land on the flight deck with smaller downstream recirculation zone. Consequently, the $M6$ model can offer a valuable reference for the design of the frigate superstructure.

It is worth noting that the flow field over the flight deck for $M6$ can be approximated to that over a backward-facing step (BFS) with a closed recirculation zone bounded by an unsteady shear layer[22], which can be seen in Fig.12[23]. For the sake of a clear description of the three-dimensional recirculation zone, a schematic of flow field over the MSFS was presented in Fig.13[24]. The recirculation zone behind the hangar appears when flow rounds the hangar. The appearance of the lateral flow from the two sides of the hangar leads to the three-dimensional flow structure over the flight deck and the appearance of the horseshoe vortex.

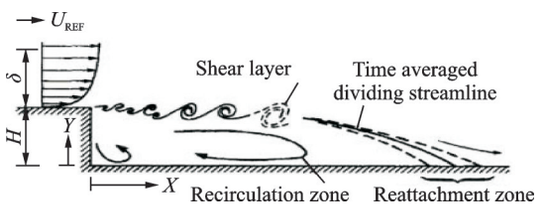

Fig.12 Flow field over backward facing step[23]

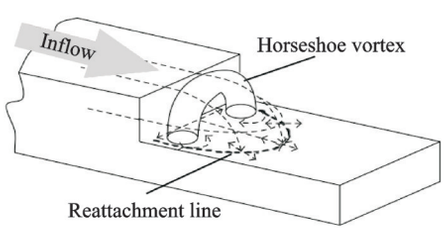

Fig.13 Flow field over simplified frigate afterbody[24]

The differences of vertical velocity for diverse MSFS models should be attracted attention while the ship-borne helicopter is operating over the deck, because the distributions of vertical velocity can influence the helicopter's safety. The distributions of velocity components at the observation line for different models were plotted in Figs.14—16, where U, V, W denote longitudinal velocity, lateral velocity and vertical velocity, respectively. The curves of longitudinal velocity are axisymmetric for

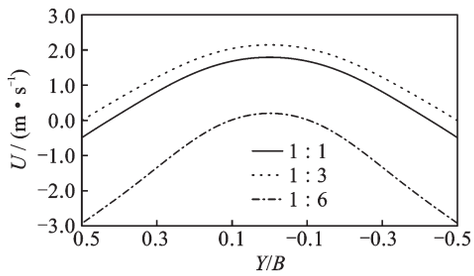

Fig.14 Distributions of longitudinal velocity at observation line

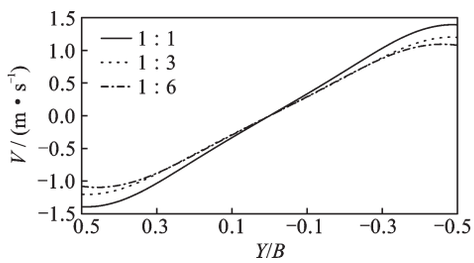

Fig.15 Distributions of lateral velocity at observation line

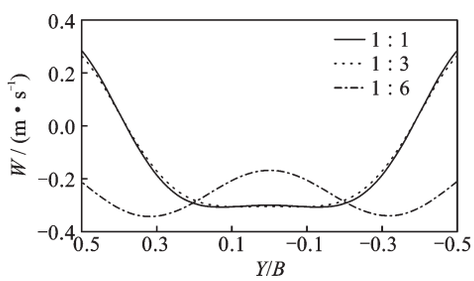

Fig.16 Distributions of vertical velocity at observation line

different models. It is worth noting that the sign of longitudinal velocity is almost positive except two sides for $M1$ and $M3$, meaning that the observation line is mainly located in the recirculation zone and the longitudinal velocity is the largest at the center for $M1$ and $M3$. However, the sign of longitudinal velocity is almost negative except the center for $M6$, meaning that the observation line is located outside the recirculation zone and the longitudinal velocity is the smallest at the center. It can be found that the distributions of lateral velocity are centrally symmetric for different models in Fig.15. In Fig.16, the downwash appears at the center and the upwash occurs on the two sides for $M1$ and $M3$. However, the observation line is only located in the downwash for $M6$.

4.2 Pitching state

In the real sea conditions, due to the random-

ness of the sea waves, the motion of the ship is more complex, which is generally irregular motion. However, some scholars assumed that the motion of the ship is simple harmonic motion to study the calculation method of the ship/helicopter operation limits envelope[25-26]. Therefore, the simple harmonic motion model was established in this paper for the MSFS models.

In the pitching state, the flow fields over different models were numerically simulated. The period of pitching motion is 2 s, the maximum pitching angle is about 5°, and the function of pitching motion is

$$\omega_y = A\cos(2\pi t/T + \theta)$$

where ω_y is the angular velocity of the rotation around the Y axis, and the unit is rad/s. In this paper, A=0.274, T=2 s, θ=0. The results of numerical simulation for different models in the third period were shown as follows.

The contours of velocity and streamlines at Map_Y for $M1$ model in pitching state were shown in Fig.17. The black points and grey points denote the center of recirculation zone and the reattachment position on the downstream wall, respectively. The tracks of their movements were illustrated in the picture. The $M1$ reaches the maximum pitching angle at $T/4$, and there is a big downstream recirculation zone similar to the flow field in the static state. The $M1$ model returns to its initial position at $T/2$ and the center of recirculation zone as well as the reattachment position gradually moves downstream. As the aft part of $M1$ is gradually sinking, the recirculation zone over the deck enlarges obviously. Moreover, the center of recirculation zone and reattachment position are moving toward the end of the deck until $3T/4$. At the end of a period, the $M1$ model returns initial position, and the center of recirculation zone as well as reattachment position is moving upstream. It can also be observed that the structure of flow fields at $T/2$ is basically the same to that at T.

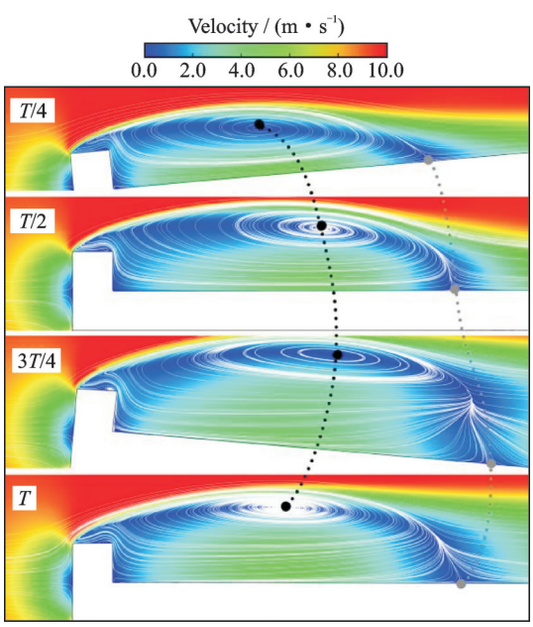

Fig.17 Contours of velocity and streamlines at Map_Y for $M1$ model in pitching state

For the $M3$ model, the tracks of the center of recirculation zone and reattachment position in a pitching period are similar to that of $M1$ model, as shown in Fig.18.

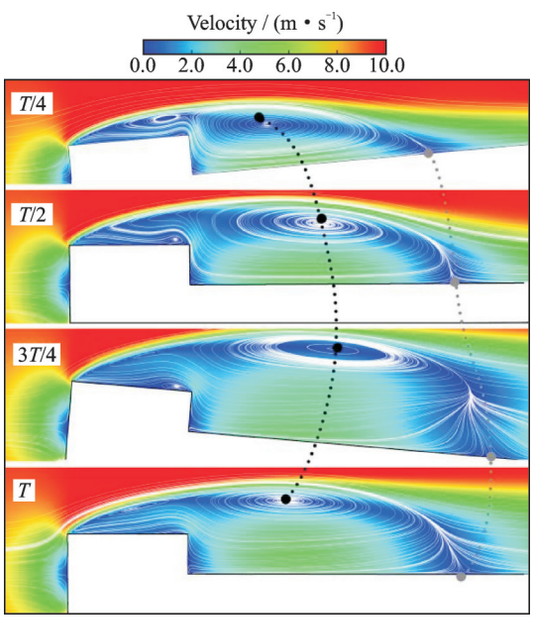

Fig.18 Contours of velocity and streamlines at Map_Y for $M3$ model in pitching state

However, there are some differences in the pitching flow fields for $M6$ compared with $M1$ and $M3$. At $T/4$, there are two big recirculation zones (upstream recirculation zone and downstream recirculation zone) over the hangar and flight deck, respectively. As the rear of the $M6$ model is gradually sinking, the upstream recirculation zone is moving downstream while the downstream recirculation zone is moving upstream. Eventually, these two re-

circulation zones are merged into one as shown in $3T/4$. When $M6$ model returns to initial position at T, the center of the merged recirculation zone is moving upstream. The location of the reattachment position is slightly moving upstream at first, then moving downstream and finally moving back to its origin in a pitching period, as shown in Fig.19.

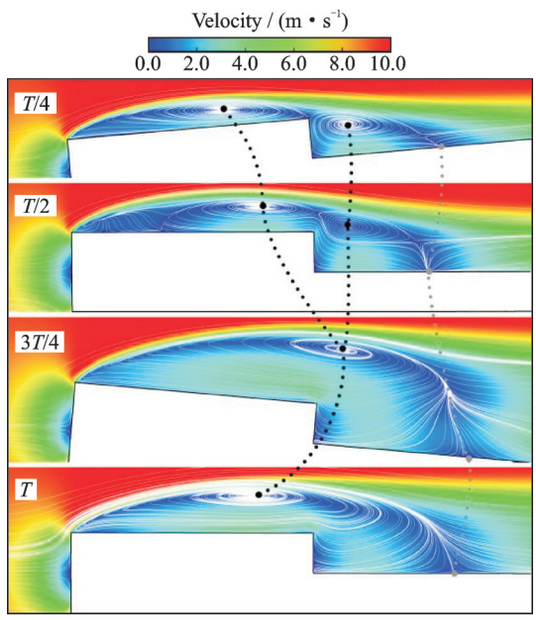

Fig.19 Contours of velocity and streamlines at Map_Y for $M6$ model in pitching state

Due to the three-dimensional characteristics of the model and flowfield, a clear description of the three-dimensional streamlines behind the hangar at different time was shown in Fig.20, where the streamlines were colored in velocity magnitude. Noting that the dominant structures of 3-D streamlines for different models are similar, therefore the 3-D streamlines for $M3$ were only presented here. It can be seen that the streamlines behind the hangar appear like a spiral shape, and keep rotating to form the recirculation zone. Compared with Fig.18, the recirculation zone also enlarges obviously as the aft part of $M3$ is gradually sinking. The motion tracks of the center of recirculation zone and reattachment position in a pitching period are similar.

In order to analyze the influence of pitching motion on the flow fields quantitatively, the velocity components at observation points in pitching state were shown in Figs.21—23. For each model the

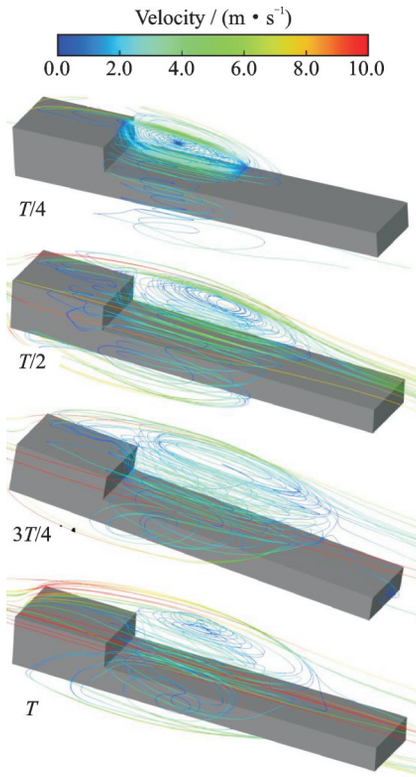

Fig.20 Schematic of 3-D streamlines for $M3$

sign of longitudinal velocity is positive, indicating that the observation point P_0 is in the backflow of recirculation zone all the time. However, the direction of longitudinal velocity at observation point P_1 is changing when MSFS is pitching, because the shear layer is swing back and forth at this point. When the point is located in the shear layer, the longitudinal velocity is close to 0. Noticeably, the longitudinal velocity at both observation points changes periodically, and the period is 2 s, which is the same as the period of the pitching motion. The variations of the longitudinal velocity are similar for $M1$ and $M3$ models, and the range of their variations is larger compared with $M6$ model.

Since the observation point P_0 is located in the central section and the MSFS models are symmetrical, the lateral velocity fluctuates slightly and is around 0 with the pitching motion. Differently, due to the observation point P_1 is not located in the central section, the lateral velocity has periodic fluctuation obviously, and the period is also 2 s.

In Fig.23(a), the direction of the vertical velocity is changing in a pitching period for $M6$ mod-

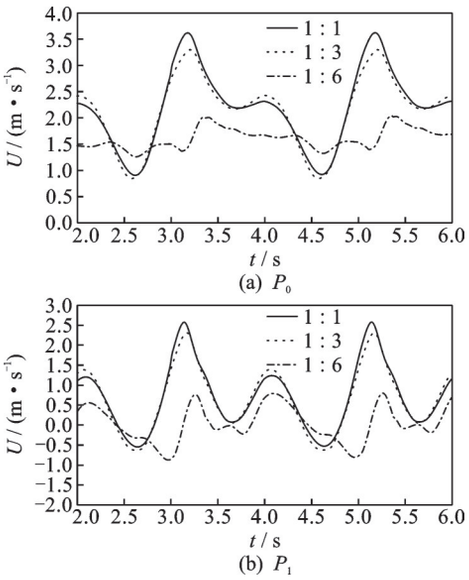

Fig.21 Curves of longitudinal velocity at different observation points in pitching state

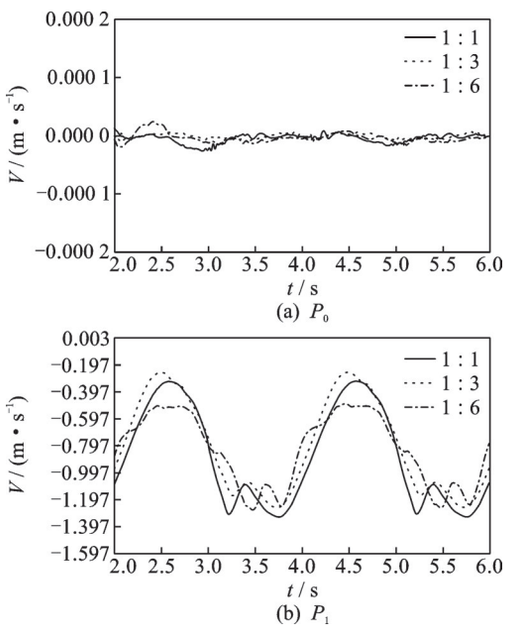

Fig.22 Curves of lateral velocity at different observation points in pitching state

el, indicating that the upwash and downwash areas are produced alternately at observation point P_0. However, for $M1$ and $M3$ models, P_0 is in the downwash area all the time and the variations of the vertical velocity are basically the same. As seen in Fig.23(b), for three different models, the upwash and downwash areas are produced alternately at observation point P_1, which is different from P_0. Similarly, the vertical velocity at these two observation points changes periodically with the periodic pitch-

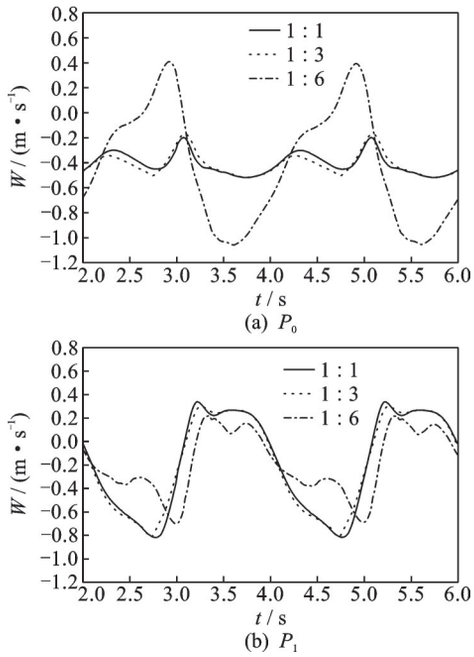

Fig.23 Curves of vertical velocity at different observation points in pitching state

ing motion, and the period is 2 s. In addition, the variations of the vertical velocity are similar for $M1$ and $M3$ models.

From the above RANS results, the periodicity of flowfield for the pitching state can be captured. For the further verification, the DES turbulence model was used in the same pitching state, due to its ability in capturing the turbulent structures for massively separated flow. The accuracy of DES is sufficient for investigating the ship airwake, and the results show better consistency with experimental data[1,17-19]. In pitching state, the vertical velocity at the observation point P_0 for $M6$ obtained from the RANS and DES methods was compared in Fig.24. The red line denotes the RANS results, and the blue line denotes the DES results. It can be found that there is obvious vertical velocity fluctuation in the DES results, so the Fast Fourier Transform was used to filter the fluctuation, and the green line denotes the filtered results. Compared with the RANS results, the vertical velocity with DES changes periodically, and the period is also about 2 s. In addition, the variations of the vertical velocity are similar for RANS and DES results. Consequently, it is reasonable to simulate the ship airwake for the ship motion case with RANS method.

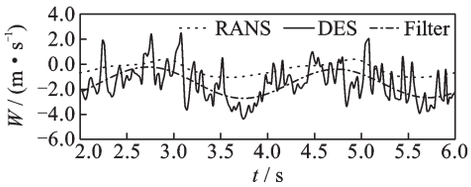

Fig.24 Comparison of RANS and DES results in pitching state for $M6$

The standard deviations of velocity components at the observation points in different models were given in Table 2 and Table 3. In Table 2, the fluctuation of longitudinal velocity at the observation point P_0 for $M1$ is larger than others. The fluctuation of the vertical velocity for $M6$ model is relatively large, while the lateral velocity in each model is almost unchanged. Compared with P_0, the standard deviation of the velocity components at P_1 is larger except the vertical velocity for $M6$, and the most obvious discrepancy exist in the lateral velocity. It also can be found in Table 3 that the standard deviations of three velocity components are the largest in $M1$, which means the flow field over the $M1$ model is more turbulent.

Table 2 Standard deviation of velocity components at observation point P_0 in pitching state m/s

Model	$M1$	$M3$	$M6$
U	0.733 9	0.682 4	0.181 7
V	0.000 0	0.000 0	0.000 0
W	0.083 4	0.090 2	0.461 5

Table 3 Standard deviation of velocity components at observation point P_1 in pitching state m/s

Model	$M1$	$M3$	$M6$
U	0.824 2	0.809 2	0.456 6
V	0.360 2	0.350 8	0.263 5
W	0.410 1	0.399 9	0.268 8

4.3 Comparisons of two states

To further analyze the differences of flow fields over the deck between pitching and static state when the MSFS model is located on the horizontal position, the comparisons of velocity components at observation point P_0 for these two states were given in Table 4 and Table 5. The subscripts "s" and "p" denote the static state and pitching state. During a pitching period, the MSFS model returns to horizontal position for two time at $T/2$ and T, and the subscripts "m" and "e" denote the middle of a period and the end of a period. Therefore, U_s, U_{pm}, U_{pe} mean the longitudinal velocity in static state, pitching state at $T/2$ and T, respectively. Δ denotes the deviation of the velocity components between two states, which is defined by $|(U_{px} - U_s)/U_{px}|$, and x can be substituted by "e" and "m".

When different models are located on the horizontal position, the velocity components have obvious divergence in different states. The longitudinal velocity in static state is lower than that in pitching state, especially for $M6$ model, the larger deviation between two states is 93.8% at $T/2$ and 94.4% at T. The reason is that in static state the observation point is located in the shear layer of $M6$, where the longitudinal velocity is very low. While the $M6$ model is in pitching motion, the recirculation zone behind the hangar is moving and increasing with the pitching motion. Therefore, the observation point is located in the backflow of the recirculation zone, where the velocity is larger. The smallest deviation occurs in $M3$ model, and the deviation between two states is 18.9% at $T/2$ and 7% at T.

The lateral velocity of the observation point P_0 approximates to 0 in static state and pitching state for different models, due to the point P_0 is located in the central section and the MSFS models are symmetrical, which is consistent with that in Fig.15 and Fig.22.

The comparisons of vertical velocity at P_0 between pitching and static states were shown in Table 5. The vertical velocity in static state is lower than that at the end of a pitching period. The largest deviation between two states appears in $M6$ model, and the deviation is 175.1% at $T/2$ and 74.5% at T. It is noteworthy that the signs of vertical velocity at $T/2$ in pitching state and static state are opposite, therefore, the deviation is more than 100%, which has the serious effect on the ship-borne helicopter because the rotor-aerodynamic force is sensitive to the upwash and downwash. The smallest deviation between two states occurs in $M1$ model, and the de-

viation is 17.4% at $T/2$ and 35.8% at T, which is relatively large and cannot be neglected for the ship-borne helicopter's safe operations over the deck. Furthermore, due to the unsteady characteristics of the instantaneous flow fields in the motion state, the velocity components at $T/2$ and T in the pitching motion is different for the same MSFS model, though the MSFS models are both located on the horizontal position at these two moments.

Table 4 Comparisons of longitudinal velocity at P_0 between pitching and static states

Model	U_s/ (m•s^{-1})	U_{pe}/ (m•s^{-1})	U_{pm}/ (m•s^{-1})	Δ_{pe}/%	Δ_{pm}/%
$M1$	1.832 6	2.317 5	2.997 7	20.9	38.9
$M3$	2.256 7	2.426 9	2.783 7	7.0	18.9
$M6$	0.094 7	1.688 2	1.527 9	94.4	93.8

Table 5 Comparisons of vertical velocity at P_0 between pitching and static states

Model	W_s/ (m•s^{-1})	W_{pe}/ (m•s^{-1})	W_{pm}/ (m•s^{-1})	Δ_{pe}/%	Δ_{pm}/%
$M1$	−0.297 5	−0.463 1	−0.253 5	35.8	17.4
$M3$	−0.299 4	−0.468 3	−0.231 7	36.1	29.2
$M6$	−0.179 2	−0.701 7	0.238 6	74.5	175.1

From Fig.25 to Fig.27, the comparisons of velocity components distributions on observation line for these two states were given to analyze the discrepancy of flow fields over the deck. Let S, P_m and P_e denote the static state, pitching state at $T/2$ and T, respectively. As shown in Fig.25, for the $M1$ model, the largest deviation of longitudinal velocity between two states appears at the center of the observation line. It is noteworthy that the deviation of the longitudinal velocity on the whole line between static state and pitching state at $T/2$ is the largest. Furthermore, the longitudinal velocity in static state is smaller than that in pitching state, and it is largest at $T/2$ in pitching state. Similarly, the largest deviation of longitudinal velocity between two states appears at the center for the $M3$ model. However, near two sides of the deck, the deviation is very small, indicating that the longitudinal velocity near the sides of deck is not affected seriously by the pitching motion. For the $M6$ model, the largest deviation of longitudinal velocity between these two states is also appearing at the center area, however, the deviation on the whole line between static state and pitching state at T moment is the largest, which is different from $M1$ and $M3$.

In Fig.26, for different models, the lateral velocity at center of the observation line is close to 0, and the deviation between two states is equal to 0, too. Nevertheless, the lateral velocity except the center has obvious deviation between two states, especially near two sides of the deck for $M6$.

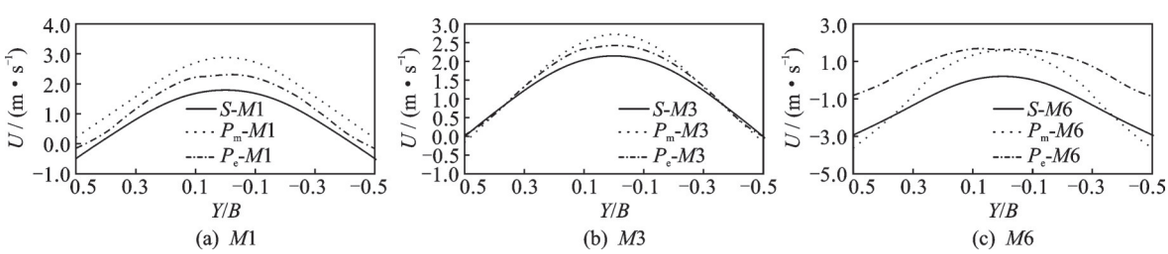

Fig.25 Comparisons of longitudinal velocity distributions at observation line for different models

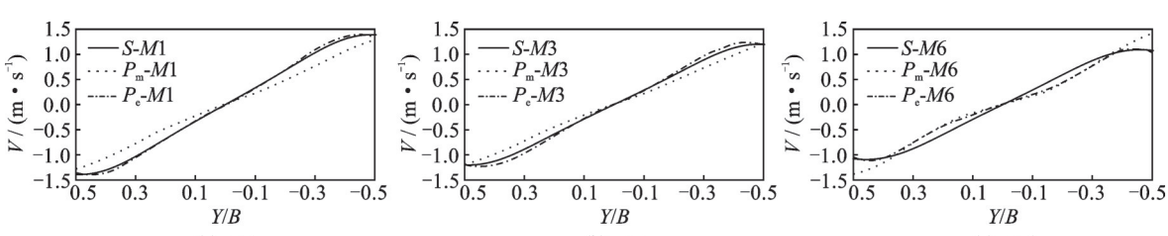

Fig.26 Comparisons of lateral velocity distributions at observation line for different models

The comparisons of vertical velocity distributions are given in Fig.27. For both $M1$ and $M3$ models, the downwash velocity in the pitching state at T is higher when $-0.2<Y/B<0.2$. The deviation of vertical velocity near two sides of the deck is relatively large between different states. When $Y/B<-0.3$ or $Y/B>0.3$, there are both upwash and downwash in the static state, however, the upwash is only appearing in the end of a pitching period and the downwash is only appearing in the middle of a pitching period. Differently, for the $M6$ model, the deviation of the vertical velocity between different states is very large, except the area near $Y/B=\pm0.25$. Particularly, at two different moments in the pitching state, the largest deviation of vertical velocity is appearing near the two sides of the deck, though the decks at two moments are both located on the same position.

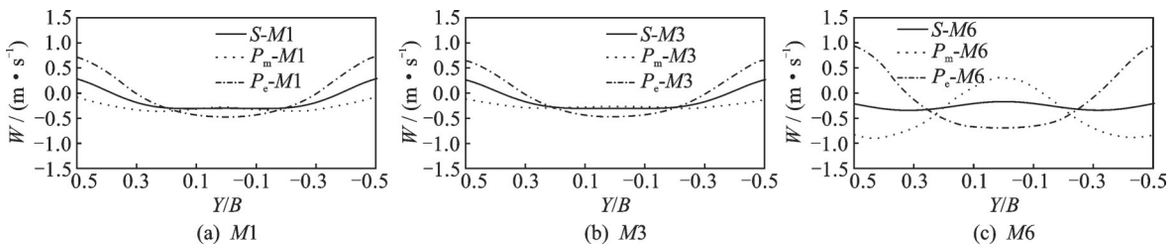

Fig.27 Comparisons of vertical velocity distributions at observation line for different models

5 Conclusions

In the current study, the numerical calculations of the unsteady flow fields over different MSFS models were carried out in the static state and pitching state, respectively, with the emphasis on the influence of ship motion on the flow fields over the flight deck. The following conclusions were obtained by comparing and analyzing the contours of velocity and streamlines, as well as the quantitative results.

(1) For different models, the structures of flow fields have obvious discrepancy. With the increase of L, the downstream recirculation zone is decreasing, which is conducive to take off and land on the deck for the ship-borne helicopter.

(2) The moving tracks of recirculation zone's center and reattachment position in a pitching period are similar in $M1$ and $M3$ models, while are different from that in $M6$ model.

(3) Except the lateral velocity at P_0, the velocity components at the observation points change periodically with the periodic pitching motion for the three models, and the period is equal to the pitching period.

(4) By comparing the deviations of the velocity components in static state and pitching state when the MSFS is located on the horizontal position, the results show that the flow field in static state is quite different from the pitching state. Therefore, the effect of ship motion cannot be neglected in analyzing ship airwake.

References

[1] FORREST J S, OWEN I. An investigation of ship airwakes using detached-eddy simulation[J]. Computers and Fluids, 2010, 39(4): 656-673.

[2] HEALEY J V. Establishing a database for flight in the wakes of structures[J]. Journal of Aircraft, 1992, 29(4): 559-564.

[3] BARDERA-MORA R. Flow field velocity on the flight deck of a frigate[J]. Journal of Aerospace Engineering, 2014, 228(G14): 2674-2680.

[4] POLSKY S A. A computational study of unsteady ship airwake[C]//Proceedings of the 40th AIAA Aerospace Sciences Meeting and Exhibit. Reno, NV: [s.n.], 2002: 1002.

[5] WOODSON S H, GHEE T A. Computational and experimental determination of the air flow around the landing deck of a U.S. navy destroyer (DDG)[C]// Proceedings of the 23rd AIAA Applied Aerodynamics Conference. Totonto, Ontario, Canada: [s. n.], 2005: 4958.

[6] THORNBER B, STARR M, DRIKAKIS D. Implicit large eddy simulation of ship airwakes[J]. Aeronautical Journal, 2010, 114(1162): 715-736.

[7] KÄÄRIÄ C H, WANG Y, WHITE M D, et al. An experimental technique for evaluating the aerodynamic impact of ship superstructures on helicopter operations[J]. Ocean Engineering, 2013, 61: 97-108.

[8] WATSON N A, KELLY M F, OWEN I, et al. Computational and experimental modeling study of the unsteady airflow over the aircraft carrier HMS Queen Elizabeth[J]. Ocean Engineering, 2019, 172: 562-574.

[9] WILKINSON C, ZAN S, GILBERT N, et al. Modeling and simulation of ship air wakes for helicopter operations—A collaborative venture[C]//Proceedings of Symposium on Fluid Dynamics Problems of Vehicles Operating Near or in the Air-Sea Interface. Amsterdam, Netherlands:[s.n.], 1998.

[10] CHENEY B T, ZAN S J. CFD code validation data and flow topology for the technical co-operation program AER-TP2 simple frigate shape: LTR-A-035[R]. [S.l.]: National Research Council of Canada, 1999.

[11] ZAN S J. Surface flow topology for a simple frigate shape[J]. Canadian Aeronautics and Space Journal, 2001, 47(1): 33-43.

[12] REDDY K R, TOFFOLETTO R, JONES K R W. Numerical simulation of ship airwake[J]. Computers and Fluids, 2000, 29(4): 451-465.

[13] SYMS G F. Simulation of simplified-frigate airwakes using a Lattice-Boltzmann method[J]. Journal of Wind Engineering and Industrial Aerodynamics, 2008, 96(6/7): 1197-1206.

[14] SPALART P R, JOU W H, STRELETS M, et al. Comments on the feasibility of LES for wings, and on a hybrid RANS/LES approach[C]//Proceedings of International Conference on DNS /LES. Ruston, Louisiana: [s.n.], 1997: 137-147.

[15] SPALART P R, DECK S, SHUR M L, et al. A new version of detached-eddy simulation, resistant to ambiguous grid densities[J]. Theoretical & Computational Fluid Dynamics, 2006, 20(3): 181-195.

[16] SHUR M L, SPALART P R, STRELETS M K, et al. A hybrid RANS-LES approach with delayed-DES and wall-modelled LES capabilities[J]. International Journal of Heat & Fluid Flow, 2008, 29(6): 1638-1649.

[17] ZHAO R, RONG J L, LI H X, et al. Entropy-based detached-eddy simulation of the airwake over a simple frigate shape[J]. Advances in Mechanical Engineering, 2015, 7(11): 1-13.

[18] LI C, JIANG W, CHENG J, et al. Comparisons of DES and LES turbulent model for simulation of surface ship airwake[C]//Proceedings of the ASME 2016 35th International Conference on Offshore Mechanics and Arctic Engineering. Busan, South Korea: [s.n.], 2016.

[19] YUAN W, WALL A, LEE R. Combined numerical and experimental simulations of unsteady ship airwakes[J]. Computers and Fluids, 2018, 172: 29-53.

[20] LI T, WANG Y B, ZHAO N, et al. An investigation of ship airwake over the frigate afterbody[J]. International Journal of Modern Physics B, 2020, 34: 2040069.

[21] GREENWELL D I, BARRETT R V. Inclined screens for control of ship air wakes[C]//Proceedings of the Third AIAA Flow Control Conference. San Francisco, CA: [s.n.], 2006: 3502.

[22] BARDERA-MORA R. Flow field velocity on the flight deck of a frigate[J]. Journal of Aerospace Engineering, 2014, 228(14): 2674-2680.

[23] DRIVER D M, SEEGMILLER H L, MARVIN J G. Time-dependent behavior of a reattaching shear layer[J]. AIAA Journal, 1987, 25(7): 914-919.

[24] BARDERA-MORA R. Experimental investigation of the flow on a simple frigate shape (SFS)[J]. The Scientific World Journal, 2014,2014: 1-8.

[25] WANG Cunren, ZHU Yubing. A study on the method of calculation for helicopter-ship take-off/landing flight envelope[J]. Flight Dynamics, 1996(1): 36-40. (in Chinese)

[26] ZHANG Xiaodong, HOU Zhiqiang, HU Gaocai, et al. Calculation of ship-helicopter operating limits envelope of a certain type of shipboard helicopter[J]. Journal of Sichuan Ordnance, 2012, 33(10): 30-33. (in Chinese)

Acknowledgements This work was supported by the Fundamental Research Funds for the Central Universities (No. NS2019006) and the Priority Academic Program Development of Jiangsu Higher Education Institutions (PAPD).

Authors Dr. **LI Tong** received the B.S. degree in mathematics from College of Science from Nanjing University of Aeronautics and Astronautics (NUAA), Nanjing, in 2016. Now he is a doctoral student majoring in computational fluid dynamics in College of Aerospace Engineering, NUAA. His research is focused on the numerical study and analysis of the flow field over the ship.

Prof. **ZHAO Ning** received his Ph.D. degree from Computing Center of Chinese Academy of Sciences in 1993. In 2000, he was appointed professor of the department of aerodynamics, NUAA. From 2001 till now, he is a doctoral su-

pervisor at the College of Aerospace Engineering, NUAA. Currently, he is the vice chairman of Chinese Aerodynamics Research Society and the standing director of the Chinese Society of Theoretical and Applied Mechanics. His research has focused on aerodynamics, computational fluid dynamics and other areas of research.

Author contributions Dr. **LI Tong** designed the study, complied the models and wrote the manuscript. Prof. **WANG Yibin** contributed to the discussion and revision of the study. Prof. **ZHAO Ning** contributed to the discussion and background of the study. All authors commented on the manuscript draft and approved the submission.

Competing interests The authors declare no competing interests.

(Production Editor: SUN Jing)

舰船运动对修改型简化护卫舰上方流场的影响

李 通,王逸斌,赵 宁

(南京航空航天大学非定常空气动力学与流动控制工业和信息化部重点实验室,南京 210016,中国)

摘要:当护卫舰向前方行进时,由于舰船的纵摇和横摇运动,其飞行甲板上方的流场变得十分复杂,可能会严重影响舰载直升机的起降。文中通过改变机库高度和长度的比例,在静止状态和纵摇状态下对不同的修改型简化护卫舰(Simple frigate shape, SFS)上方的流场进行了数值研究,该SFS模型由机库和飞行甲板组成。对于不同的模型,对比分析了静止状态和纵摇状态下,飞行甲板上方的速度和压力云图,以及观测点和观测线上的速度分量变化。结果显示,不同模型中回流区的大小和再附点的位置有着明显的不同,同时揭示了在一个周期性纵摇运动中,回流区中心和再附位置的轨迹变化。另外,两个观测位置的速度分量也随着舰船运动产生了周期性变化。而且,静止状态和纵摇状态下的速度分量差异相当大,因此,静止状态下的流场不能准确的模拟纵摇状态下的流场。

关键词:计算流体力学;简化护卫舰外形;舰船尾流;纵摇;回流区